Postprint of: Wang K., Liu S., Wang L., Smulko J., Wen H., Novel Interpolation Method of Multi-DFT-Bins for Frequency Estimation of Signal with Parameter Step Change, IEEE TRANSACTIONS ON INSTRUMENTATION AND MEASUREMENT Vol. 71 (2021), 6500914, DOI: 10.1109/TIM.2021.3139652

Novel Interpolation Method of Multi-DFT-Bins for Frequency Estimation of Signal with Parameter Step Change

Kai Wang, Shan Liu, Lanlan Wang, Janusz Smulko and He Wen

***Abstract*—The IpDFT(Interpolation Discrete Fourier Transform) method is one of the most commonly used non-parametric methods. However, when a parameter(frequency, amplitude or phase) step changes in the DFT period, the DFT coefficients will be distorted seriously, resulting in the large estimation error of the IpDFT method. Hence, it is a key challenge to find an IpDFT method, which not only can eliminate the effect of the step-changed symbol, but also can sufficiently eliminate the fence effect and the spectrum leakage. In this paper, an IpDFT based method is proposed to estimate the frequency of the single tone signal with the step-changed parameters in the sampling signal sequence. The relationship between the DFT bins and the step changed parameters is given by several linear equations. At most six different DFT bins are used to eliminate the effect of symbol.**

***Index Terms*—Interpolation Discrete Fourier Transform (DFT); frequency estimation; the single tone signal; step-changed parameter; RF conformance test.**

I. Introduction

With the development of signal processing technology, frequency estimation plays an increasingly important role in this field. A large number of parametric methods (time-domain methods) the non-parametric methods (frequency-domain methods) have emerged in the past few decades. For example, the ML (Maximum likelihood) method [1], [2], the Wavelet method [3], the filtering method [4], [5], PLL (Phase locked loop) method [6], prony method [7], Taylor Fourier Filter method [8], [9] and the IpDFT method (the interpolation Discrete Fourier Transform).

The IpDFT method and its improvements, such as the e-IpDFT [10] and i-IpDFT [11], which can be simplified by the Fast Fourier Transform (FFT), is currently one kind of the most commonly used non-parametric methods [12], [13]. The DFT-based estimators are fast and very simple to apply [14], [15]. For the single tone signal, the IpDFT methods have completely solved the estimation error caused by the fence effect. With two or three DFT bins, various IpDFT methods [16]–[18] are proposed to estimate the frequency of the signal. For the real-value harmonic signal, the most important challenge is how to compensate for spectrum leakages, which heavily damages the estimation accuracy [19]–[22]. Many variants of DFT, such as Sliding DFT [23], Taylor Fourier Filter method [8], [9], Iterative IpDFT [24] and Frequency Shifting Filtering [25], have been reported to estimate the phasor parameters. All of these methods try to compensate for spectrum leakages, which are caused by the off-nominal frequency operation of the system.

In the IpDFT method, windowing techniques such as the maximum decay sidelobe window [26], [27] and the triangular self-convolution window [28] are also used to reduce harmonic and inter-harmonic interference. Besides windowing techniques, another method is to consider the contribution of each frequency component in the spectrum and to solve the spectrum leakage problem theoretically. [29], [30] completely eliminate the influence of spectrum leakage by a three-point IpDFT based on MDW. Furthermore, the authors of [30] apply the algorithm of [29] to the harmonic signal. Other authors [31], [32] propose an IpDFT based on a scaling factor to estimate the dominant chatter frequency. Based on the rectangular window, [33]–[35] introduce an efficient two-point/three-point IpDFT of the sinusoid signal with or without the damping factor. [36], [37] combine the CLS (complex-value least squares) criteria and SDFT (Smart DFT) to obtain higher algorithm accuracy.

The default signal model in IpDFT methods is the time invariant signal, which means the amplitude, phase and frequency of the signal remain unchanged during the sampling period. However, the time-varying signals also have research significance in real-world scenarios. For example, the basic of RF conformance testing system is a fast and accurate frequency offset estimation method for the wireless systems with different modulation signals, such as quadrature amplitude modulation signal (QAM), phase-shift keying signal (PSK) and frequency-shift keying signal (FSK) [38], [39]. QAM signal, PSK signal and FSK signal can be regarded as carrier signals whose amplitude, phase and frequency vary with the transmission information during different sampling cycles [40], [41]. In the power systems, the precise and rapid frequency estimation is also necessary in PMUs (phasor measurement units) [42], [43]. The standards of phasors estimation provide detailed test requirements for the time-varying signal, including step change in amplitude, phase and frequency

This work was supported in part by the National Key Research and Development Program of China under Grant 2020YFC2004003 and Grant 2020YFC2004002, the National Natural Science Foundation of China under Grant 61771190 and in part by the Natural Science Foundation of Hunan Province under Grant 2019JJ20001.

Kai Wang, Shan Liu and Lanlan Wang are with the School of Information Science and Engineering, Southeast University, 9 Mozhoudonglu, Jiangning District, Nanjing 211111, China(e-mail: kaiwang@seu.edu.cn; Jasmine_63@163.com; wanglanlan_12138@163.com).

Janusz Smulko is with Gdansk University of Technology, Poland

He Wen is with the College of Electrical and Information Engineering, Hunan University, Changsha, Hunan Province(e-mail: he_wen82@126.com)

This article has been accepted for publication in a future issue of this journal, but has not been fully edited. Content may change prior to final publication. Citation information: DOI 10.1109/TIM.2021.3139652, IEEE Transactions on Instrumentation and Measurement

[44]–[46]. However, the research of IpDFT based frequency estimation for the time-varying signal frequency estimation is still in the preliminary stage. Others [47] propose a low complexity IpDFT method to estimate frequency offset for M-QAM coherent optical systems. A novel IpDFT frequency estimation method of single tone signal with bit transition is proposed in [48].

The signals with step-changed parameters are the most important and basic signal modes in the wireless system [40], [41] or the power system [44]–[46]. The basic algorithms, which are utilized in the RF conformance test [38], [39] or in the phasor measurement units [42], [43], are also used for the frequency estimation in different signal modes. A rapid and accurate estimation can greatly ensure reliable performance of the test system. However, when a parameter step changes in the DFT period, the DFT coefficients will be distorted seriously, resulting in the large estimation error of the IpDFT method. Hence, it is a key challenge to find an IpDFT method, which not only can eliminate the effect of the step-changed symbol, but also can sufficiently eliminate the fence effect and the spectrum leakage. In this paper, an IpDFT based method is proposed to estimate the frequency of the single tone signal with the step-changed parameter in the sampling signal sequence. The relationship between the DFT bins and the step-changed parameters is given by several linear equations. At most six different DFT bins are used to eliminate the effect of the step-changed parameters. The results of simulation and experiment confirm that the proposed algorithm can achieve frequency estimation with high accuracy.

II. Frequency Estimation Method

A single tone signal with the step-changed parameters can be described as

$$\begin{aligned} x(n) &= s(n) + q(n) \\ &= A_m \exp(\varphi_m) \exp(j\omega_m n) + q(n) \end{aligned} \tag{1}$$

where A_m, φ_m and $\omega_m = 2\pi f_m T_s$ are the m-th ($m \in [0, M-1)$) unknown parameters of the amplitude, the phase and the angular frequency. $q(n)$ is the additive white Gaussian noise (AWGN) with variance σ_q^2. f_m is the signal frequency and T_s is the sampling time.

When we obtain an N-sample time sequence $x(n)$, we rewrite the symbols of the m-th jump as U_m and ω_m where $\omega_m = 2\pi l_m/N = 2\pi(k_m + \delta_m)/N$, l_m is the m-th acquired signal cycles. $\delta_m \in [-0.5, 0.5]$ and $k_m \in \left[0, 1, \cdots, \frac{N}{2} - 1\right]$ are the fractional-part and the integer-part of l_m. The N-point DFT of $x(n)$ is:

$$\begin{aligned} X(k) &= \sum_{n=0}^{N-1} s(n) W_N^{nk} + \sum_{n=0}^{N-1} q(n) W_N^{nk} \\ &= S(k) + Q(k) \end{aligned} \tag{2}$$

where $W_N^k = e^{-j\left(\frac{2\pi}{N}\right)k}$, $S(k)$ and $Q(k)$ are the DFTs of $s(n)$ and $q(n)$.

A. the case when the frequency, the amplitude and the phase all step change

In this part, we only consider the case of one step-change in an N-length signal. Let the parameters(frequency, amplitude or phase) step change on the L-th sample. The angular frequency before the step-change is denoted as ω_1 and the angular frequency after the step-change is denoted as ω_2:

$$s(n) = \begin{cases} U_1 e^{j\omega_1 n}, & n = 0, 1, \cdots, L-1 \\ U_2 e^{j\omega_2 n}, & n = L+1, L+2, \cdots, N-1 \end{cases} \tag{3}$$

where $U_1 = A_1 \exp(\varphi_1)$ and $U_2 = A_2 \exp(\varphi_2)$ are any two different unknown parameters of amplitude and phase combination. The DFT result at slot k changes to:

$$\begin{aligned} S(k) &= \sum_{n=0}^{L-1} A_1 e^{j\varphi_1} e^{j\omega_1 n} W_N^{nk} + \sum_{n=L}^{N-1} A_2 e^{j\varphi_2} e^{j\omega_2 n} W_N^{nk} \\ &= A_1 e^{j\varphi_1} \frac{1 - \left(e^{j\omega_1} W_N^k\right)^L}{1 - e^{j\omega_1} W_N^k} + A_2 e^{j(\varphi_2 + L\omega_2)} W_N^{kL} \frac{1 - \left(e^{j\omega_2} W_N^k\right)^{N-L}}{1 - e^{j\omega_2} W_N^k} \\ &= A_1 e^{j\varphi_1} \frac{1 - \left(e^{j\omega_1} W_N^k\right)^L}{1 - e^{j\omega_1} W_N^k} + A_2 e^{j\varphi'_2} W_N^{kL} \frac{1 - \left(e^{j\omega_2} W_N^k\right)^{N-L}}{1 - e^{j\omega_2} W_N^k} \\ &= \frac{(p_1 + p_2) + (q_1 + q_2) W_N^k + (u_1 + u_2) W_N^{kL} + (v_1 + v_2) W_N^{k(L+1)}}{1 - (\lambda_1 + \lambda_2) W_N^k + \lambda_1 \lambda_2 W_N^{2k}} \end{aligned} \tag{4}$$

where $\lambda_1 = e^{j\omega_1}$, $\lambda_2 = e^{j\omega_2}$, $p_1 = A_1 e^{j\varphi_1}$, $p_2 = -A_2 e^{j\varphi'_2} e^{j\omega_2 L}$, $q_1 = -A_1 e^{j\varphi_1} e^{j\omega_2}$, $q_2 = A_2 e^{j\varphi'_2} e^{j(\omega_1 + \omega_2(N-L))}$, $u_1 = -A_1 e^{j\varphi_1} e^{j\omega_1 L}$, $u_2 = A_2 e^{j\varphi'_2}$, $v_1 = A_1 e^{j\varphi_1} e^{j(\omega_2 + \omega_1 L)}$, $v_2 = -A_2 e^{j\varphi'_2} e^{j\omega_1}$ and $\varphi'_2 = \varphi_2 + L\omega_2$. The coarse frequency estimation can be performed as: $\hat{k}_0 = \arg \max_{k \in \{0,1,\ldots,N-1\}} (|X(k)|)$. When we get any six different DFT bins $\mathbf{X}(k) = [X(k_1), X(k_2), \cdots, X(k_6)]^T$, we can get the following linear equations according to (4):

$$\mathbf{X}_k = \mathbf{W}_k \eta \tag{5}$$

where η and $\mathbf{W}_k$ can be written as:

$$\eta = [p_1 + p_2, q_1 + q_2, u_1 + u_2, v_1 + v_2, \lambda_1 + \lambda_2, \lambda_1 \lambda_2]^T \tag{6}$$

$$\mathbf{W}_k = \begin{bmatrix} 1 & W_N^{k_1} & W_N^{k_1 L} & W_N^{k_1(L+1)} & X(k_1) W_N^{k_1} & -X(k_1) W_N^{2k_1} \\ 1 & W_N^{k_2} & W_N^{k_2 L} & W_N^{k_2(L+1)} & X(k_2) W_N^{k_2} & -X(k_2) W_N^{2k_2} \\ 1 & W_N^{k_3} & W_N^{k_3 L} & W_N^{k_3(L+1)} & X(k_3) W_N^{k_3} & -X(k_3) W_N^{2k_3} \\ 1 & W_N^{k_4} & W_N^{k_4 L} & W_N^{k_4(L+1)} & X(k_4) W_N^{k_4} & -X(k_4) W_N^{2k_4} \\ 1 & W_N^{k_5} & W_N^{k_5 L} & W_N^{k_5(L+1)} & X(k_5) W_N^{k_5} & -X(k_5) W_N^{2k_5} \\ 1 & W_N^{k_6} & W_N^{k_6 L} & W_N^{k_6(L+1)} & X(k_6) W_N^{k_6} & -X(k_6) W_N^{2k_6} \end{bmatrix} \tag{7}$$

According to Eq.(5), η can be estimated as:

$$\hat{\eta} = \mathbf{W}_k^{-1} \mathbf{X}_k \tag{8}$$

where $\hat{\cdot}$ is the estimated value of (.). Let $\hat{\lambda}_1 + \hat{\lambda}_2 = a$ and $\hat{\lambda}_1 \hat{\lambda}_2 = b$, where a and b are calculated from Eq. (6). ω_1 and

This article has been accepted for publication in a future issue of this journal, but has not been fully edited. Content may change prior to final publication. Citation information: DOI 10.1109/TIM.2021.3139652, IEEE Transactions on Instrumentation and Measurement

ω_2 can be estimated as:

$$\begin{cases} \hat{\omega}_1 = \dfrac{\mathrm{Im}\left(\ln\left(a + \sqrt{a^2 - 4b}\right)\right)}{2} \\ \hat{\omega}_2 = \dfrac{\mathrm{Im}\left(\ln\left(a - \sqrt{a^2 - 4b}\right)\right)}{2} \end{cases} \tag{9}$$

Although any of the six different DFT bins can be used in our method, it is recommended to use the DFT bins with the six largest magnitudes to obtain the best estimation results in practical applications.

B. the case when the amplitude and the phase step change, but the frequency keeps unchange

In this part, we keep the frequency constant, and let the amplitude and the phase step change during the sampling signal sequence. In order to distinguish the frequency step chage of part A, ω_0 is chosen to represent the signal angular frequency. Eq.(4) can be simplified as:

$$\begin{aligned} S\left(k\right) &= \sum_{n=0}^{L-1} A_1 e^{j\varphi_1} e^{j\omega_0 n} W_N^{nk} + \sum_{n=L}^{N-1} A_2 e^{j\varphi_2} e^{j\omega_0 n} W_N^{nk} \\ &= A_1 e^{j\varphi_1} \frac{1 - \left(e^{j\omega_0} W_N^k\right)^L}{1 - e^{j\omega_0} W_N^k} + A_2 e^{j\varphi'_2} W_N^{kL} \frac{1 - \left(e^{j\omega_0} W_N^k\right)^{N-L}}{1 - e^{j\omega_0} W_N^k} \\ &= \frac{\left(\mu_1 - \nu_2\right) + \left(\mu_2 - \nu_1\right) W_N^{kL}}{1 - \lambda_0 W_N^k} \end{aligned} \tag{10}$$

where $\mu_1 = A_1 e^{j\varphi_1}$, $\mu_2 = A_2 e^{j\varphi'_2}$, $\nu_1 = A_1 e^{j\varphi_1} (\lambda_0)^L$, $\nu_2 = A_2 e^{j\varphi'_2} (\lambda_0)^{N-L}$ and $\lambda_0 = e^{j\omega_0}$. When we get any three different DFT bins $\mathbf{X}_k = \left[X\left(k_1\right), X\left(k_2\right), X\left(k_3\right)\right]^T$, $\eta = \left[\mu_1 - \nu_2, \mu_2 - \nu_1, \lambda_0\right]^T$ can be estimated as:

$$\hat{\eta} = \mathbf{W}_k^{-1} \mathbf{X}_k \tag{11}$$

where

$$\mathbf{W}_k = \begin{bmatrix} 1 & W_N^{k_1 L} & X\left(k_1\right) W_N^{k_1} \\ 1 & W_N^{k_2 L} & X\left(k_2\right) W_N^{k_2} \\ 1 & W_N^{k_3 L} & X\left(k_3\right) W_N^{k_3} \end{bmatrix} \tag{12}$$

ω_0 can be estimated as:

$$\hat{\omega}_0 = \mathrm{Im}\left(\ln \hat{\lambda}_0\right) \tag{13}$$

In this condition, the DFT bin with the largest magnitude and its adjacent DFT bins: $X\left(k_0\right)$, $X\left(k_0 + 1\right)$, $X\left(k_0 - 1\right)$ are recommended in practical applications for better estimation results.

C. Estimation Method of the location of bit transition L

The actual location of bit transition L is important in the proposed algorithm according to Eq. (4) and Eq. (10). In the calculation process, if the value of L is wrong, it will cause the frequency estimation error. In Refs. [47], [48], L is set to a known value by default. However, it is not always an easy job because it is simply impossible to know the transition time beforehand in any measurement. If L is unknown, we can use a sliding window based time-frequency estimation to get the value of L. Assuming the signal of length $N = 128$, the step-change of parameter occurs at an unknown point L. We choose a rectangular window with a window size of $N' = 64$ and a step length of 1. By using this rectangular window, we divide the signal into 65 data frames. The frame length and the frame shift of each data frame are 64 and 1, respectively. For the any m-th data frame: $\{x\left(m - 63\right), x\left(m - 1\right), \cdots, x\left(m\right)\}$, the IpDFT method given in [16] is used to is used to estimate the frequency $\omega\left(m\right)$ of the m-th data frame. The estimation results for the step-changed signals when SNR=40dB are shown in Figure 1. As shown in Fig. 1(a), the amplitude and the phase jump point appears at 7-th point and 71-st point, which means the location of bit transition L is 7. We can also use 71-64=7 to obtain the same result. As shown in Fig. 1(b), the frequency jump point appears at the point as same as the Fig. 1(a) and it obtains the same result.

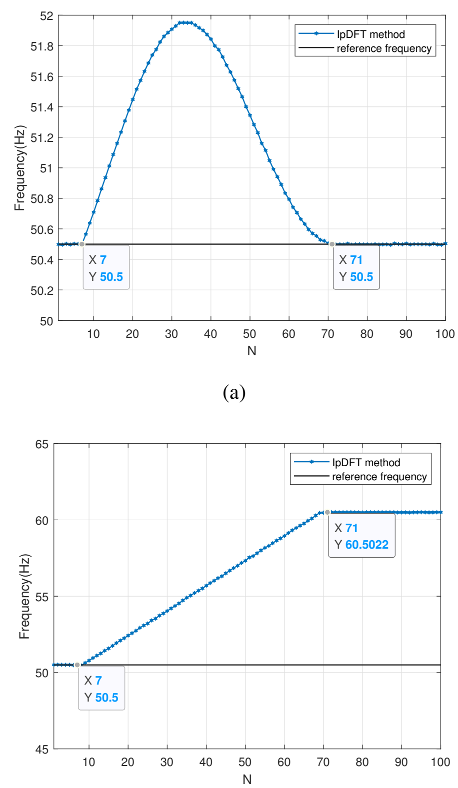

(a)

(b)

Fig. 1: The sliding window based time-frequency estimation (a) the step-change of the amplitude and the phase; (b) the step-change of the frequency

The sliding window method can be utilized as a coarse estimation of the location L. Furthermore, we will analyze the effect of transition time error in the frequency estimation and discuss its impact in this paper. We denote the estimated location by the coarse estimation as L' and then we can get a set L consisting of L' and its neighbors:L=$\{\cdots .L' - 2, L' - 1, L', L' + 1, L' + 2, \cdots\}$. With the elements in set L in turn, we estimate ω according to the method proposed in section II and denote the estimated values as: $\omega\left(\mathrm{L}\right) =$

This article has been accepted for publication in a future issue of this journal, but has not been fully edited. Content may change prior to final publication. Citation information: DOI 10.1109/TIM.2021.3139652, IEEE Transactions on Instrumentation and Measurement

TABLE I: MSEs of $\hat{\omega}$ with different sampling points in different conditions(unit: dB)

L	**60**	**61**	**62**	**63**	**64**	**65**	**66**	**67**	**68**	**69**	**70**
Condition: the step-change of the amplitude and the phase											
noiseless	-68.6849	-74.9372	-85.5932	-101.7746	-320.2516	-82.0556	-72.7839	-66.9066	-62.5740	-59.1483	-56.3269
SNR=40dB	-68.5969	-74.9061	-83.1398	-85.5546	-86.8574	-80.4095	-72.7481	-66.9098	-62.5128	-59.1237	-56.3227
SNR=15dB	-61.1405	-61.2445	-62.1591	-61.3460	-60.5947	-61.1215	-61.2578	-60.4537	-59.6906	-57.9072	-54.7129
Condition: the step-change of the frequency											
noiseless	-37.6932	-40.5259	-44.3341	-50.5133	-254.3888	-50.1606	-43.4749	-38.9035	-35.0644	-31.6950	-28.7563
SNR=40dB	-37.6995	-40.5325	-44.3040	-50.5135	-76.8406	-50.1302	-43.4625	-38.9028	-35.0705	-31.6894	-28.7464
SNR=15dB	-36.9852	-38.0281	-42.3912	-40.3862	-41.1338	-44.3340	-42.7269	-38.7947	-34.9241	-31.823	-28.7188

$\{\cdots, \omega(L'-2), \omega(L'-1), \omega(L'), \omega(L'+1), \omega(L'+2), \cdots\}$. In Tab. I, we calculate the MSEs (The mean square error) between the actual frequency of signal ω and the estimated frequencies with different location ω(L) in noiseless/ noisy condition.

There are two factors that affect the estimation accuracy of our method. One is the value of SNR. The other is the value of L'. In the low noise environment, the influence of the value of L' is more important. As shown in Tab. I, we can accurately estimate ω when the value of L' is right($L' = L$) When the value of L' is wrong($L' \neq L$), our method is a biased estimation algorithm. The estimation error will gradually increase with the increasing of the difference between L and L'. In the high-noise environment, the influence of SNR is more important. The influence of the error L', whose value is slightly different from the real value L, can be ignored in the estimation process. We can get the estimated values with little differences even we use the wrong L' when SNR=15dB.

Furthermore, we calculate the differences between two adjacent estimated frequencies according to Eq. (14). The results in the noiseless and the low noise condition are shown in Figure 2 and Figure 3. We set $L = 64$, $N = 128$ and L=$\{60, 61, 62, 63, 64, 65, 66, 67, 68, 69, 70\}$. As shown in Fig.2, when the value of L' is equal to the actual value L the difference between $\omega(L)$ and adjacent estimated frequencies $\omega(L-1)$ is the maximum.

$$\mathrm{diff}(i) = 10\log_{10}|\omega(i) - \omega(i-1)| \, (i \in L) \tag{14}$$

In this paper, our main research purpose is to reveal the relation between the DFT bins and the system parameters of the signal with step-changed parameters, which allows us to better understand the essence of discrete Fourier transform. The research on the estimation of the location L is only at early stage. So far, we haven't given the explicit expression between the DFT bins and the location L in this paper. In our future work, we will focus on this issue for further research and discussion.

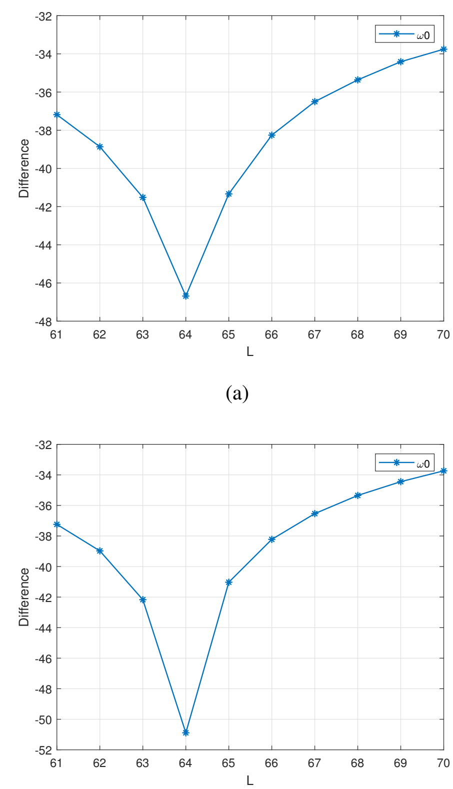

(a)

(b)

Fig. 2: the difference between two adjacent estimated frequencies when the amplitude and the phase step change a) SNR=40dB; b) noiseless

III. Performance of Proposed Method

In this section, we focused on analyzing the estimation performance of the algorithm without any practical application. The normalized angular frequency ω_i is chosen in this part, where $\omega_i = 2\pi l_i/N = 2\pi f_i/f_s \ (i = 0, 1 \text{ or } 2)$.

We compare the estimated performance of the considered algorithm through simulation results. The considered algorithms are the XJX method in Ref. [47], the UFE method in Ref. [48], the BFEL method in Ref. [48], the ITE-FOE method in Ref. [49], the DIFF-FOE method in Ref. [50]. Cramer-Rao lower bounds (CRLB) is shown in Eq.(14).

$$\mathrm{CRLB}(\omega_0) \geq \frac{12\sigma^2}{A^2 N (N^2 - 1)} \tag{15}$$

where A is the amplitude of the signal, N is the signal length and σ^2 is the variance of the additive white Gaussian noise.

The observed sample length N is 128. For each parameter, 3000 runs are performed to evaluate the statistical properties. The mean square error (MSE) is used to evaluate the performance of the proposed estimator and other algorithms, which is given by:

$$\mathrm{MSE} = 10\log_{10}\left(\frac{1}{M}\sum_{i=1}^{M}(\hat{\omega}(i) - \omega)^2\right) \tag{16}$$

where $\hat{\omega}(i)$ presents the estimated frequency of the i-th independent simulation.

This article has been accepted for publication in a future issue of this journal, but has not been fully edited. Content may change prior to final publication. Citation information: DOI 10.1109/TIM.2021.3139652, IEEE Transactions on Instrumentation and Measurement

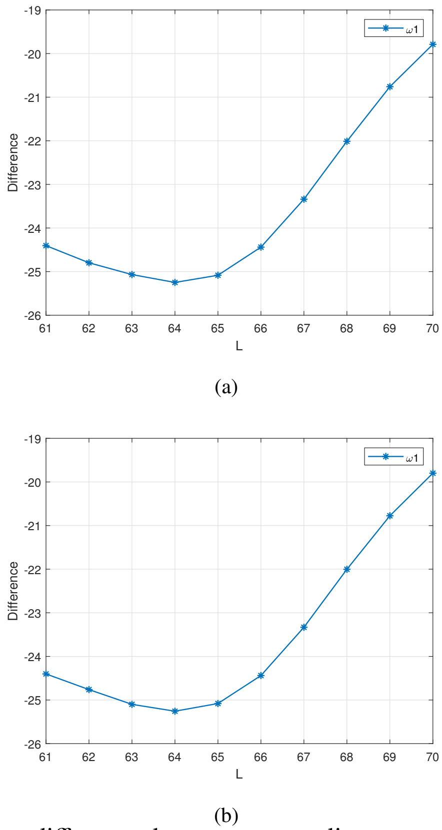

Fig. 3: the difference between two adjacent estimated frequencies when the amplitude and the phase step change a) SNR=40dB; b) noiseless

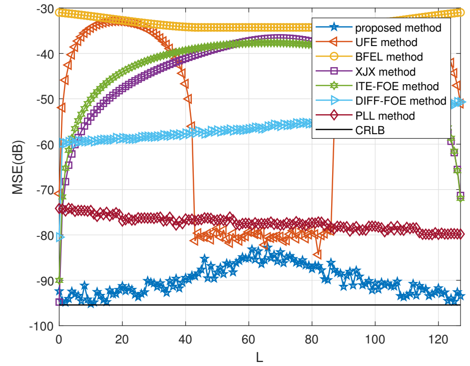

Fig. 4: MSEs of $\hat{\omega}_0$ versus L with l_0=1.06 and SNR=40dB

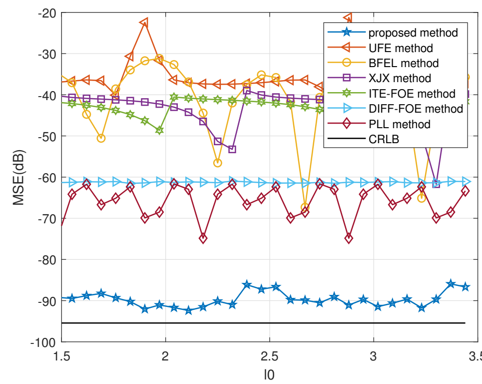

Fig. 5: MSEs of $\hat{\omega}_0$ versus l_0 with SNR=40dB and L=32

A. the case when the amplitude and the phase step change, but the frequency keeps unchanged

Firstly, let's consider the case when the amplitude and the phase step change, but the frequency keeps unchanged. The jumping point L of our algorithm can be applied to [0, N-1]. When $L = 0$ or $N-1$, the signal actually degenerates into a single-frequency complex exponential signal, and our method actually degenerates into an IpDFT method in [16]–[18]. We set $U_1 = 0.9\exp(10\pi/180)$ and $U_2 = \exp(80\pi/180)$. Figure 4 depicts the relationships between L and MSEs in the noisy environment. Set l_0=1.06 and let L change from 0 to 127. As shown in Fig. 4, our method acheives better performance. However, the UFE method only performs well when the jump point L is in the interval $[N/3\,, 2N/3\,]$. Furthermore, let's take L=32 as an example to analyze the performances of our method with different l_0 or SNR.

Figure 5 depicts the relationships between l_0 and MSEs when SNR=40dB and L=32. Then, let l_0 change from 0.5 to 3.5. As shown in Fig. 5, our method can achieve the minimum MSE -90dB. However, the minimum MSE of UFE is only –35dB, which means the performance of our method is much better than that of UFE method when SNR=40dB and L=32. Fig. 6 depicts the relationships between SNR and MSEs when L=32. Set l_0=1.06 and let SNR change from 0dB to 40dB. The MSEs of our method decrease linearly when SNR increases, which means that our methods can estimate the frequency correctly when amplitude and phase step change on L–th sample. However, UFE method can only estimate the frequency correctly when $L \in [N/3\,, 2N/3\,]$. In order to verify the effect of different sampling points N on the estimated frequency, set l_0=1.06 and SNR=40dB. The MSE of frequency is shown in Table II, and the results show that our method has better effect under different sampling points N when L=32.

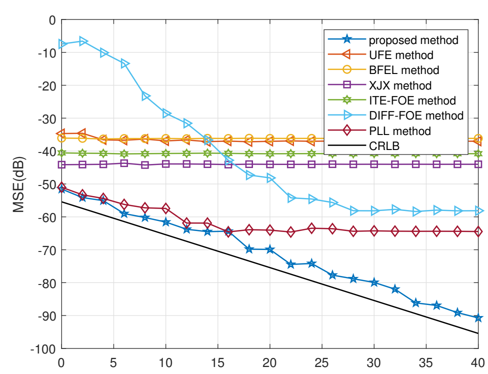

Fig. 6: MSEs of $\hat{\omega}_0$ versus SNR with l_0=1.06 and L=32

Let's consider the case when the signal is distorted by the DC offset or the harmonics. The signal distorted by the DC

This article has been accepted for publication in a future issue of this journal, but has not been fully edited. Content may change prior to final publication. Citation information: DOI 10.1109/TIM.2021.3139652, IEEE Transactions on Instrumentation and Measurement

TABLE II: MSEs of $\hat{\omega}_0$ with different sampling points N when L = 32 (unit: dB)

		Proposd Method	UFE Method	BFEL Method	XJX Method	ITE-DFT	DIFF-DFT	PLL
L=32	N=128	-83.53	-36.27	-34.19	-42.45	-39.39	-56.38	-76.34
	N=256	-92.98	-38.16	-38.59	-55.05	-50.63	-63.20	-81.16
	N=512	-101.51	-46.13	-43.72	-67.28	-62.74	-69.79	-86.23
	N=1024	-108.92	-56.42	-49.34	-79.42	-75.21	-76.25	-91.78

TABLE III: Condition of fundamental and harmonics

Harmonic	1st	3rd	5th	7th	9th	11th	13th	15th
Amplitude(rms)	0	-26.02	-33.97	-42.14	-53.18	-66.22	-78.26	-90.30

offset can be expressed as:

$$\begin{aligned} x(n) &= s(n) + q(n) \\ &= A_m \exp(\varphi_m) \exp(j\omega_m n) + A_{dc} + q(n) \end{aligned} \tag{17}$$

where $A_{dc} = 1$. Let $X_{dc}(k)$ be the DFT of the signal A_{dc}. When $k > 0$, the value of $X_{dc}(k) = 0$. In practical applications, if we do not use $X_{dc}(0)$ in estimation process, we can reduce the DC offset interference. The performances distorted by the DC offset are shown in Fig. 7. Set L=32 and SNR = 40dB. Our method can correctly estimate the frequencies no matter the DC offset distorted or not.

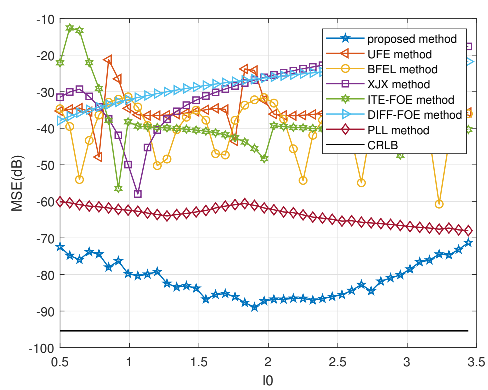

Fig. 7: MSEs of $\hat{\omega}_0$ versus l_0 with SNR=40dB, A_{dc} = 1 and L=32

The signal distorted by noise and the 2-8 harmonics can be expressed as:

$$\begin{aligned} x(n) &= s(n) + q(n) \\ &= A_m \exp(\varphi_m) \exp(j\omega_m n) \\ &+ \sum_{h=2}^{8} A_p \exp(j\omega_h n + \varphi_h) + q(n) \end{aligned} \tag{18}$$

where A_h are shown in Table III [42], [43]. φ_h is the initial phase which are selected at random in the range $[0, 2\pi)$. Due to the influence of harmonics, the overall estimation effect of our algorithm becomes less satisfactory as shown in Fig. 8.

B. the case when the frequency, the amplitude and the phase all step change

Let's consider the case when the frequency, the amplitude and the phase all step change when $U_1 = 0.9 \exp(10\pi/180)$ and $U_2 = \exp(80\pi/180)$. Set $l_1 = l_2 + 0.5$. As shown in Fig. 9, our method achieve the minimum MSE -75dB when L=64 and SNR=40dB. Fig. 10 illustrates that the MSEs of our

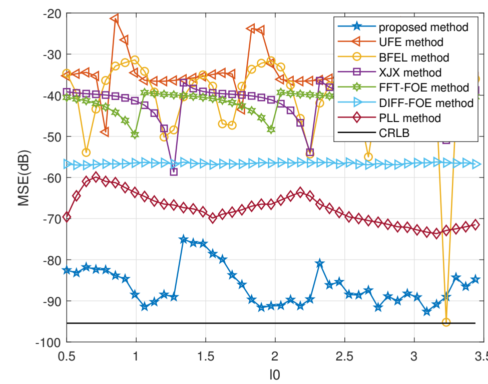

Fig. 8: MSEs of $\hat{\omega}_0$ versus l_0 distorted by 2-7 harmonics with SNR=40dB and L=32

method decrease linearly when SNR increases, which means only our methods can estimate the frequency accurately with a step change in the frequency of the signal. As shown in Fig. 11, when $40 < L < N-3$, our method can estimate l_1 accurately. When $2 < L < 80$, our method can estimate l_2 accurately. Besides, our method achieves the minimum MSE -75dB when L=64 is in the interval[50, 100]. Therefore, our method has a better performance when L is in the interval [3, N–4] in the case that the frequency step change. The reason for L taking this interval is as follows. In our algorithm, the signal sequence with step-changed frequency is equivalent to a signal sequence formed by splicing two single-frequency complex exponential signals with different frequencies. For single-frequency complex exponential signals, at least two consecutive samples of $s(n)$ and $s(n+1)$ can accurately estimate the corresponding frequency. In other words, for a single-frequency complex exponential signal, at least two samples are required to fully describe it. Our algorithm considers two single-frequency complex exponential signals jointly. Simulation shows that for each single-frequency complex exponential signal, at least three consecutive samples are required to fully describe its complete information. Therefore, the variation range of L is actually $[3, N-4]$. When $L < 3$, the frequency of ω_1 cannot be estimated; when $L > N-4$, the frequency of ω_2 cannot be estimated.

In order to verify the effect of different sampling points N on the estimated frequency, Set l_1=1.5, l_2=0.5 and SNR=40dB. The MSE of frequency is shown in Table IV, and the results show that our method has better effect under different sampling points N when $L = \frac{N}{2}$.

The signal distorted by the DC offset is shown in Fig. 12

This article has been accepted for publication in a future issue of this journal, but has not been fully edited. Content may change prior to final publication. Citation information: DOI 10.1109/TIM.2021.3139652, IEEE Transactions on Instrumentation and Measurement

TABLE IV: MSEs of $\hat{\omega}_1$ and $\hat{\omega}_2$ with different sampling points N when $L = \frac{N}{2}$ and SNR = 40dB(unit: dB)

		Proposed Method	UFE Method	BFEL Method	XJX Method	ITE-DFT Method	DIFF-DFT Method	PLL Method
N=128	l_1	-72.54	-49.51	-54.64	-29.56	-14.93	-34.65	-64.56
	l_2	-70.04	-26.28	-26.00	-23.33	-16.79	-35.71	-
N=256	l_1	-81.68	-54.04	-60.21	-35.63	-21.19	-40.70	-67.84
	l_2	-80.39	-32.40	-32.04	-29.37	-23.13	-41.71	-
N=512	l_1	-90.63	-59.33	-65.94	-41.67	-27.34	-46.74	-71.12
	l_2	-89.29	-38.43	-38.0	-35.40	-29.33	-47.67	-
N=1024	l_1	-98.73	-65.08	-71.84	-47.70	-33.43	-52.74	-76.78
	l_2	-98.93	-44.48	-44.05	-41.43	-35.43	-53.70	-

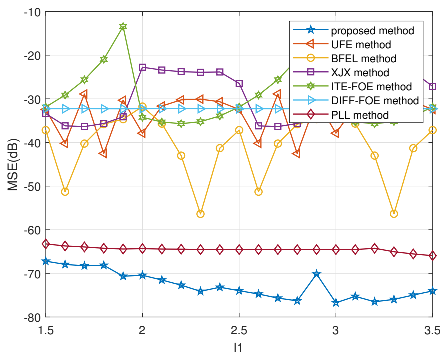

(a)

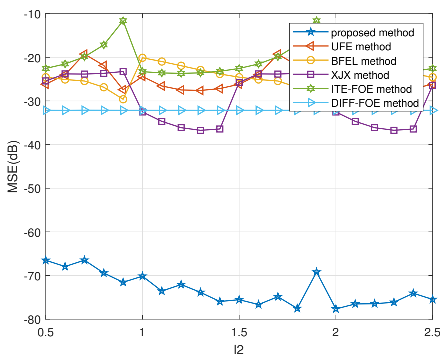

(b)

Fig. 9: The relationships between $l_i\,(i = 1, 2)$ and MSEs of $\hat{\omega}_1$ and $\hat{\omega}_2$ when SNR=40dB and $L = 64$ (a) l_1; (b) l_2

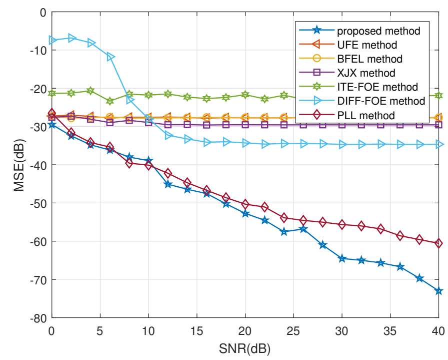

(a)

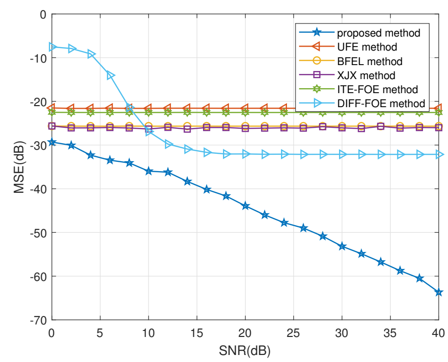

(b)

Fig. 10: The relationships between SNR and MSEs of $\hat{\omega}_1$ and $\hat{\omega}_2$ when l_1 =1.5, l_2 =0.5 and L=64 (a) l_1; (b) l_2

and the signal distorted by the harmonics of part A is shown in Fig. 13.

C. Computational Complexity

We give the computational complexity analysis of our method. As shown in Eq. (12), three different DFT bins $X(k)$ are needed to establish the equation for the amplitude or phase jump signal. The evaluation of one DFT sample requires N complex multiplications and N-1 complex additions. To compute the frequency parameters, we need a 3×3 complex matrix inverse operation. If the Gauss elimination method is used, the evaluation of 6×6 matrix inversion requires $\sum_{p=1}^{6} p \times p$ complex multiplications and $\sum_{p=0}^{5} p \times p$ complex additions. Therefore, the overall complexity of the proposal is $PN + \sum_{p=1}^{P} p \times p$ complex multiplications and $P(N-1) + \sum_{p=0}^{P-1} p \times p$ complex additions. P=5 for the case when the frequency step changes and P=3 for the case when the amplitude and the phase both step change.

IV. PMU Test

In the power systems, we select 50.5 Hz as the reference frequency, 5800 Hz as the sampling frequency and the length of the signal sequence is 128 and the specific frequency is denoted as $f_i\,(i = 0, 1, 2)$. Eq. (1) is often used to describe the balanced three-phase voltage signal by means of the Clark transform [51]. In power system, the step changes of amplitude, phase and frequency are the three important conditions which should be considered. Therefore, the basis of

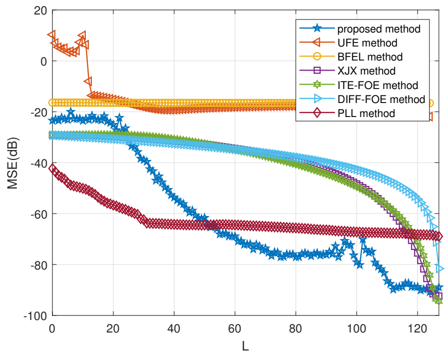

(a)

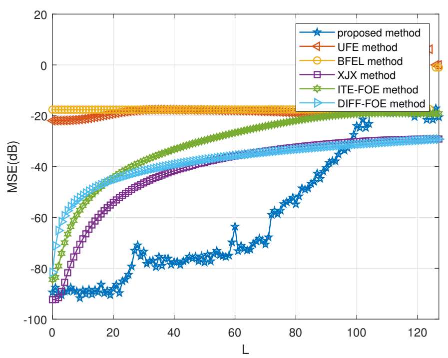

(b)

Fig. 11: The relationships between L and MSEs of $\hat{\omega}_1$ and $\hat{\omega}_2$ when l_1 =1.5, l_2 =0.5 and SNR=40dB (a) l_1; (b) l_2

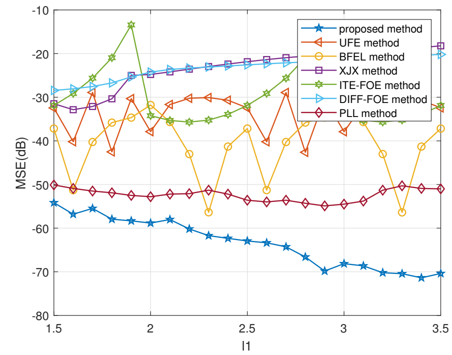

(a)

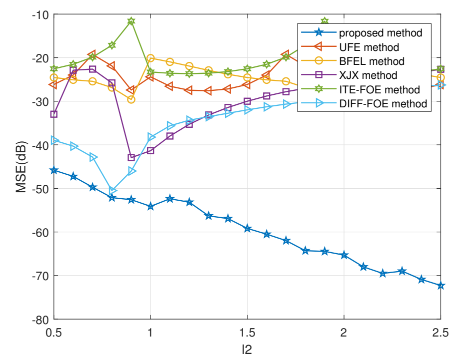

(b)

Fig. 12: The relationships between (a)l_1 and (b)l_2 and MSEs of $\hat{\omega}_1$ and $\hat{\omega}_2$ with SNR=40dB, A_{dc} = 1 and L=64

the power quality assessment is a fast and accurate frequency estimation method under an abrupt signal step.To evaluate the dynamic response when exposed to an abrupt signal change, a positive step followed by a reverse step back to the starting value under various conditions is applied to the amplitude, phase angle, and frequency of the signal, respectively.

A. Results Under the Parameters Step Signal Condition

Firstly, let's consider the case when the amplitude and the phase step change, and the frequency keeps unchanged. Fig. 14 and Fig. 15 show the results of simulation for step change signals in the magnitude and the phase with SNR=40dB. The magnitude step size is set to 0.1, and the phase step size is set to $\pi/18$. Step changes occur at t = 0.15 sec and are released at t = 0.3 sec. The proposed algorithm follows the reference frequency even when the step change occurs and is released. The PLL algorithm can also estimate the frequency well under the condition that the frequency keeps constant. The simulation results of Fig. 14 and Fig. 15 show that the MSE of the PLL algorithm can reach -76.56dB and -79.78dB, respectively. Our algorithm mse can roughly reach -95.18dB and -98.05dB before and after the step change. However, the UFE algorithm can accurately estimate ω_0 for step change signals in the magnitude or the phase only when the jump point L is in the interval [44,86].

Fig. 16 and Fig. 17 show the performances of our method for the signal with step-changed frequency in the noiseless or noisy environment. The dynamic response of our algorithm needs to be discussed respectively. The reference frequency 50.5 Hz changes to 60.5 Hz at t = 1 sec and is released at t = 2 sec. When the jump point $L < 88$, our algorithm can accurately estimate ω_1. When the jump point $L > 40$, our algorithm can accurately estimate ω_2. When the jump point L is in the interval $L \in [41, 88]$, our algorithm can accurately estimate ω_1 and ω_2 at the same time.

For the N-sample signal with the step-changed magnitude and phase, the total length of signal with the angular frequency ω_0 keeps the length of N unchanged. The information of the angular frequency ω_0 always exists in the N sampling points. Therefore, when L is the interval $[0, N-1]$, as shown in Fig. 14 and Fig. 16, the estimation accuracy of the algorithm remains unchanged. For the N-sample signal with the step-changed frequency, the information of ω_1 only contains the first L sampling points and the information of ω_2 only contains the last $N-L$ sampling points. For the signal with length N, with the increase of the L, the influence of ω_1 in observation sequence is greater, and the anti-noise perform of ω_1 is better. The smaller L is, the greater the influence of ω_2 in observation sequence is, and the better the anti-noise perform ω_2 is. Therefore, as shown in Fig. 16, the estimated performance of ω_1 will be improved with the increase of L. The estimated performance of ω_2 will be improved with the decrease of L. The sampling frequency is set to 1800 Hz. In our method, rise time occurs when t = 1.0011s (L = 126), peak time

This article has been accepted for publication in a future issue of this journal, but has not been fully edited. Content may change prior to final publication. Citation information: DOI 10.1109/TIM.2021.3139652, IEEE Transactions on Instrumentation and Measurement

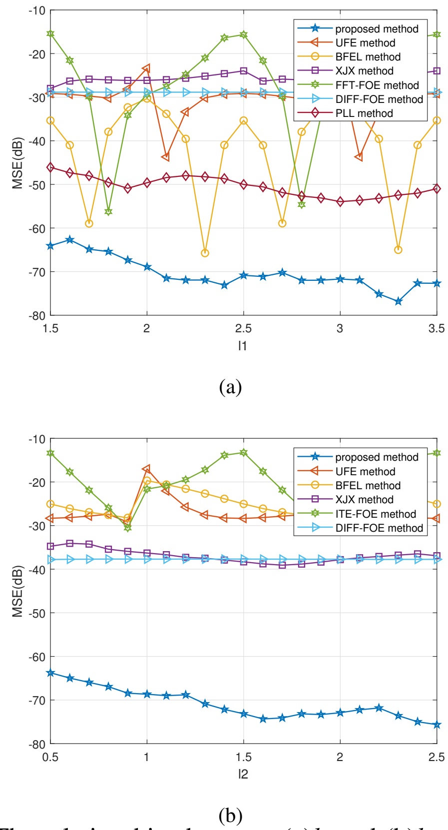

Fig. 13: The relationships between (a)l_1 and (b)l_2 distorted by 2-7 harmonics and MSEs of $\hat{\omega}_1$ and $\hat{\omega}_2$ with SNR=40dB and L=64

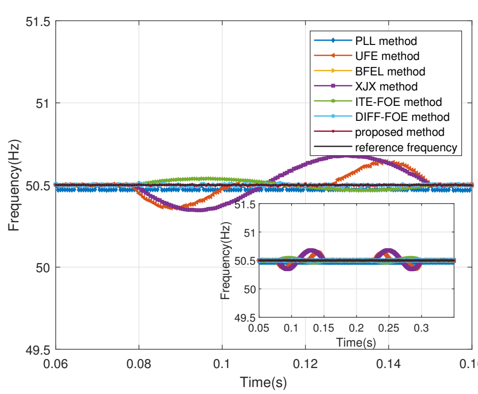

Fig. 14: The estimated frequencies of simulation for step change signals in the magnitude when SNR=40dB.

occurs when t = 1.0089s (L = 112), and adjustment time occurs when t = 1.0221s (L = 88). The overshoot has reached 79.2% according to Eq. (18). For the PLL method, rise time occurs when t = 1.0094s (L = 111). Peak time occurs when t = 1.0128s (L = 105) respectively. The overshoot has reached 9.4%.

$$\frac{X_{\max} - X(\infty)}{X(\infty)} \times 100\% \tag{19}$$

where $X_{\max}$ represents the instantaneous maximum deviation of the adjustment value, and $X(\infty)$ represents the steady-state value.

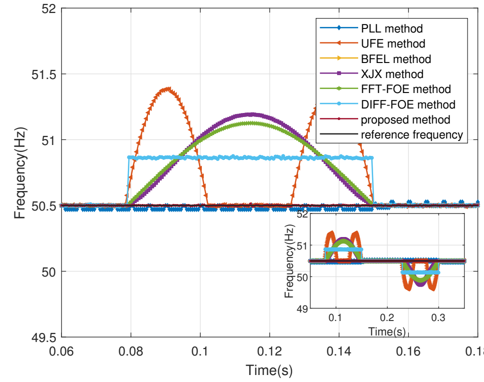

Fig. 15: The estimated frequencies of simulation for step change signals in the phase when SNR=40dB.

It can be observed from Fig. 17 that the minimum MSE of ω_1 and ω_2 can reach -122.58dB and -161.51dB when L = 3 in the noiseless environment respectively. Within the allowable error range, there is neither overshoot nor undershoot. When the sampling frequency is set to f_s, the rise time, peak time and adjustment time are all $3/f_s$. To sum up, the PLL can quickly achieve frequency tracking of the step signal in the noisy environment. However, our method has a larger maximum error in the noisy environment. However, it has a considerable advantage that the angular frequencies ω_1 and ω_2 before and after the frequency step change can be calculated simultaneously.

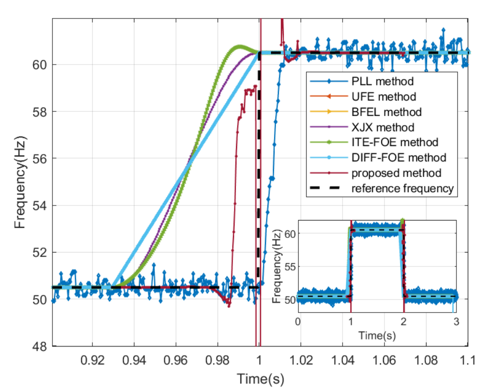

Fig. 16: The estimated frequencies of simulation for step change signals in the frequency when SNR=40dB.

B. Results Under IEEE C37.118.-2014 Standard

This section presents the simulation results of P-Class and M-Class synchrophasor measurements for the power system with 50.5 Hz signal frequency. According to IEEE C37.118.-2014 standard, the estimated performances of various algorithms are compared with an amplitude modulated signal, a phase modulated signal and a ramp signal. Eq. (20) gives the

This article has been accepted for publication in a future issue of this journal, but has not been fully edited. Content may change prior to final publication. Citation information: DOI 10.1109/TIM.2021.3139652, IEEE Transactions on Instrumentation and Measurement

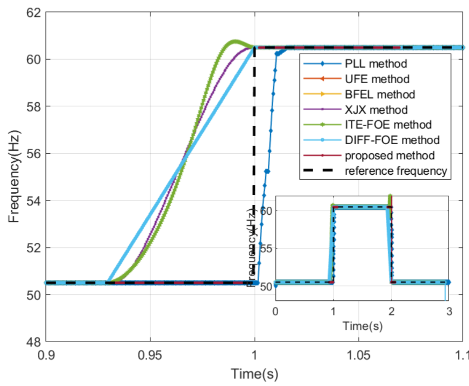

Fig. 17: The estimated frequencies of simulation for step change signals in the frequency under noiseless conditions.

amplitude modulated and phase modulated signal and Eq. (21) gives the chirp signal.

$$X_1 = A\left[1 + \alpha \cos\left(2\pi f_1 t\right)\right] \times \cos\left[2\pi f_0 t + \beta \cos\left(2\pi f_1 t - \pi\right)\right] \tag{20}$$

$$X_2 = A_1 e^{j\left(2\pi f_1 t + \pi R_f t^2\right)} \tag{21}$$

The frequency error ($|FE|$), the total vector error (TVE) and rate of change of frequency (ROCOF) are used as the index to evaluate the performance of the considered methods. $|FE|$, TVE and ROCOF are defined as follows:

$$|\mathrm{FE}| = \left|\hat{f} - f\right| \tag{22}$$

$$\mathrm{TVE} = \sqrt{\frac{\left(\hat{A}_r - A_r\right)^2 + \left(\left(\hat{A}_i - A_i\right)\right)^2}{\left(A_r\right)^2 + \left(A_i\right)^2}} \times 100\% \tag{23}$$

$$\mathrm{ROCOF} = \frac{\hat{f}(n) - \hat{f}(n-1)}{T_{RR}} \tag{24}$$

where $\hat{A}_r$ and $\hat{A}_i$ are the real and imaginary parts of the estimated amplitude, A_r and A_i are the real and imaginary parts of the true amplitude, $\hat{f}$ is the estimated frequency and f is the true frequency of the signal. $T_{RR} = 1/f_{RR}$ and f_{RR} is the PMU reporting rate.

We will divide this part of simulation into two parts according to section III. The initial parameters are all set as N = 128 and f_s = 6400 Hz. The average values and max values of $|FE|$, TVE and ROCOF of all the considered methods will be shown in the following six tables.

1) Amplitude modulation signal: In the first case when the amplitude and the phase step change when the frequency keeps unchanged, β is set to 0. α is set to -0.1 and 0.1 respectively before and after the step change. 0.2 per unit amplitude variation with 1.0 Hz of frequency is applied to the single-stone signaland the system frequency is set to 50.5Hz. The average values of |FE|, TVE and ROCOF of all the compared methods are shown in Table V-VII. In the second case when the frequency, the amplitude and the phase all step change, the frequency is set to 50.5 Hz and 20.8 Hz respectively before and after the step change. Other parameters remain unchanged in the first case. The estimated results are shown in Table VIII-X.

2) Phase modulation signal: In the first case when the amplitude and the phase step change, α is set to 0. β is set to -0.1 and 0.1 respectively before and after the step change. Modulation frequency and system frequency are referred to the amplitude modulated signal shown above. The average values of |FE|, TVE and ROCOF of all the compared methods are shown in Table V-VII. In the second case when the frequency, the amplitude and the phase all step change and the frequency is set to 50.5 Hz and 20.8 Hz respectively before and after the step change. Other parameters remain unchanged in the first case. The estimated results are shown in Table VIII-X.

3) Ramp signal: In the first case when the amplitude and the phase step change, the positive ramp rate is 1.0 Hz/ sec and the negative ramp rate is -1.0 Hz/ sec. The amplitude before and after the step change is set to 1 and 0.9 respectively. The estimated results are shown in Table V-VII. In the second case when the frequency, the amplitude and the phase all step change, and the frequency is set to 50.5 Hz and 20.8 Hz respectively before and after the step change. Other parameters remain unchanged in the first case. The estimated results are shown in Table VIII-X.

V. Experimental Verification

In this section, we will demonstrate the advantages of our method in actual conditions. Eq. (1) can be used to describe the modulation signals in the wireless systems, such as quadrature amplitude modulation signal (QAM), phase-shift keying signal (PSK) and frequency-shift keying signal (FSK) [40], [41]. QAM signal, PSK signal and FSK signal are the most widely used modulation modes in communication.

We select the WLAN RF conformance testing, which is the most conformed one in the field of IM. The WLAN RF conformance testing has been widely used in the practical application. The channel environment in the WLAN RF conformance testing is simple and idealized. Most interferences in the actual wireless communication can be ignored during the testing. Engineers of the RF conformance testing choose the method in Ref. [50], which is also compared in this paper, to estimate the carrier frequency offset(COF).

"NI WLAN Analysis" is a wireless RF conformance test system developed by National Instruments [52]. This test system provides the functions of signal generation and analysis for the test application of WLAN 802.11a/b/g/j/p/n/ac/ax/be. One of the most important functions of this test system is to judge whether the test results of the DUT(device under test) meet the test standard. A typical SISO test platform is shown in Fig. 18. Part ③ is the DUT, which is a wireless router supporting 802.11 ax. The output interfaces of the DUT is connected directly to the input interfaces of the RF conformance tester through a green specific cables, which is the part ④ in Fig. 18. The MIMO test scenario can be regarded as several SISO testers working in parallel. Keeping the physical connection form between the DUT and the tester unchanged, we can assemble a MIMO system with several same SISO systems. As the test system should be placed in a microwave anechoic chamber to avoid noise interference, the communication model in the RF test system is simple

This article has been accepted for publication in a future issue of this journal, but has not been fully edited. Content may change prior to final publication. Citation information: DOI 10.1109/TIM.2021.3139652, IEEE Transactions on Instrumentation and Measurement

TABLE V: Average |FE| (Hz) of all comparative methods

	Proposed	UFE	BFEL	XJX	ITE-DFT	DIFF-DFT	PLL
Off-nominal frequencies	0.016	0.512	19.189	0.256	0.189	0.053	0.021
Harmonic distortions	0.215	10.806	8.539	6.958	6.235	5.322	0.256
Amplitude modulation	0.015	1.074	20.310	0.548	0.307	0.038	0.019
Phase modulation	0.026	1.798	19.222	1.028	1.009	0.840	0.030
Positive ramp	0.062	8.083	0.556	0.056	0.069	0.061	0.066
Negative ramp	0.062	0.052	0.629	0.071	0.058	0.061	0.065

TABLE VI: Average TVE(%) of all comparative methods

	Proposed	UFE	BFEL	XJX	ITE-DFT	DIFF-DFT	PLL
Off-nominal frequencies	0.783	4.420	24.861	3.974	2.543	1.179	0.831
Harmonic distortions	0.059	0.165	0.062	0.212	0.145	0.197	0.064
Amplitude modulation	0.105	4.863	20.093	4.316	2.249	0.324	0.167
Phase modulation	0.074	12.714	82.722	10.064	9.855	8.061	0.079
Positive ramp	0.004	0.010	0.004	0.096	0.026	0.013	0.009
Negative ramp	0.006	0.129	0.844	0.038	0.020	0.011	0.011

TABLE VII: ROCOF estimator

	Proposed	UFE	BFEL	XJX	ITE-DFT	DIFF-DFT	PLL
Amplitude modulation	0.003	0.008	0.003	0.002	0.010	0.010	0.005
Phase modulation	0.003	0.011	0.002	0.003	0.002	0.009	0.005
Positive ramp	0.004	0.010	0.005	0.004	0.002	0.013	0.006
Negative ramp	0.004	0.008	0.004	0.003	0.002	0.013	0.006

and idealistic, where the specific cable is used to connect the communication link. Testers do not need to consider the signal attenuation and distortion caused by various interferences in actual wireless communication, such as multipath effects.

"NI WLAN Analysis Soft Front Panel" is shown in Fig. 19. With the zero-IF technique, 2.4G Hz WLAN signal is received and down converted to baseband signal. After synchronization, the I/Q measurement, carrier frequency estimation and demodulation, the tester calculates the EVM (Error Vector Magnitude) to evaluate the RF performances of DUT. As shown in Fig.19, the COF is an important index in RF conformance test. According to the test requirement, the tester needs to measure the frequency offset of each subcarrier. Under this test requirement, only the subcarrier to be tested is allowed to transmit signals, and the remaining subcarriers are prohibited from transmitting signal. The tester can control the DUT to complete the above functions with the AT command.

In summary, the communication model in the RF test system is simple and idealistic. The state-of-the-art methods, which can be used in the high-speed digital communication networks, are not needed to the algorithm engineers of RF conformance testing. On the contrary, although they aren't applicable for the actual wireless communication, the methods in Refs. [49], [50] and our method are suitable for the RF conformance testing. Let's take 802.11 ax as an example. The transmission power and the receiving power used in "NI WLAN Analysis" are 10dBm and 20dBm. The line loss is about 3dBm. Then bandwidth of 802.11 ax signal is 20 MHz. The sampling frequency is set $f_s = 1.25 \cdot$bandwidth = 25MHz. With the zero-IF technique, the 2.4G Hz 802.11ax signal is received and down converted to baseband signal. Without the carrier frequency offset, the frequency points of subcarriers in baseband are 0Hz, $20/K$ Hz, $40\mathrm{M}/K$ Hz......, where K is the total number of subcarriers. When frequency offset exists, the frequency point

TABLE VIII: Average |FE| (Hz) of all comparative methods

		Proposed	UFE	BFEL	XJX	ITE-FOE	DIFF-FOE	PLL
Off-nominal frequencies	ω_1	0.182	18.972	19.995	9.656	35.404	8.853	0.235
	ω_2	0.268	25.214	24.191	39.343	65.091	20.834	-
Harmonic distortions	ω_1	1.082	18.167	18.976	17.047	19.062	2.232	1.131
	ω_2	2.232	22.386	22.243	26.322	28.546	24.327	-
Amplitude modulation	ω_1	0.006	3.103	2.781	3.900	2.728	3.528	0.011
	ω_2	0.003	4.083	3.405	0.588	1.415	1.159	-
Phase modulation	ω_1	0.016	3.860	2.101	3.838	2.534	3.919	0.021
	ω_2	0.011	3.326	4.086	6.526	6.222	5.768	-
Positive ramp	ω_1	0.031	0.251	0.261	0.199	0.426	0.106	0.036
	ω_2	0.031	0.598	0.423	0.440	0.728	0.354	-
Negative ramp	ω_1	0.031	0.293	0.259	0.189	0.254	0.168	0.036
	ω_2	0.032	0.575	0.425	0.386	0.540	0.292	-

This article has been accepted for publication in a future issue of this journal, but has not been fully edited. Content may change prior to final publication. Citation information: DOI 10.1109/TIM.2021.3139652, IEEE Transactions on Instrumentation and Measurement

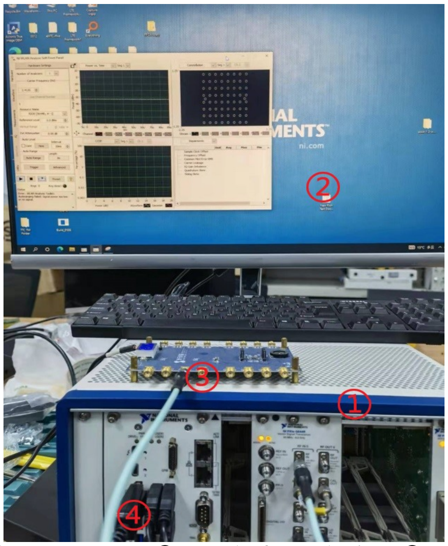

Fig. 18: The test system ①test platform device; ②screen; ③the DUT(device under test); ④the input interfaces through cables.

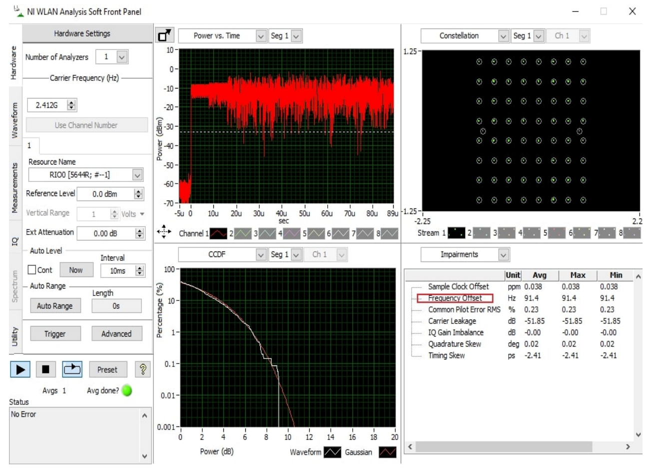

Fig. 19: NI WLAN Analysis Soft Front Panel.

of k-th subcarrier is $\Delta f_k + k\frac{20}{K}$MHz, where$\Delta f_k$ is the frequency offset and its value is no more than 100Hz. We select the 0-th subcarrier as the research object and set the frequency offset as 91.4Hz. The 64-QAM signals are sent by the DUT and measured by "NI WLAN Analysis". We cooperate with algorithm engineers of NI to give a performance comparison in the case that the two adjacent symbols jump, when N = 128 and L = 64. The comparison results are shown in Table XI. Our method can accurately estimate the frequency in the two-symbol combination scenario. When the difference between the two symbols is large (such as $U_1 = 1 + j$ and $U_1 = 1 + 7j$), the method proposed in [50] can still estimate the actual carrier. In addition, if we select the first 64 sample points of the signal, the signal is a single carrier signal with the constant amplitude, frequency and phase. At this time, the carrier can be accurately estimated by Refs. [49], [50]. The MSEs of the two algorithms in noise-free are -312dB and -337dB. The MSEs of the two algorithms in "NI WLAN Analysis" are -87dB and -85dB. Therefore, in the noisy state, if we select the 64-point sampling point corresponding to a symbol for the estimation in Refs. [49], [50], the estimation results are respectively close to and slightly worse than the estimation result obtained by our algorithm with 128 adjacent sampling points of two different symbols.

TABLE IX: Average TVE(%) of all comparative methods

		Proposed	UFE	BFEL	XJX	ITE-FOE	DIFF-FOE	PLL
Off-nominal	ω_1	0.313	12.225	10.102	19.697	28.236	17.040	0.358
frequencies	ω_2	0.155	1.082	0.502	0.609	5.366	0.757	-
Harmonic	ω_1	2.531	14.057	11.203	18.011	21.272	12.599	2.582
distortions	ω_2	2.543	14.172	13.543	19.432	24.212	13.122	-
Amplitude	ω_1	0.116	12.077	10.000	21.449	17.429	19.048	0.162
modulation	ω_2	0.078	35.462	7.456	46.934	16.657	22.939	-
Phase	ω_1	1.224	16.028	10.000	19.072	19.848	21.520	1.269
modulation	ω_2	1.843	16.553	19.037	31.641	22.159	25.062	-
Positive	ω_1	0.010	1.240	0.830	0.337	5.369	0.567	0.015
ramp	ω_2	0.154	1.082	0.502	0.609	5.366	0.756	-
Negative	ω_1	0.350	1.687	0.884	0.475	0.467	0.837	0.403
ramp	ω_2	0.991	1.418	0.600	0.749	0.715	0.635	-

TABLE X: ROCOF estimator

		Proposed	UFE	BFEL	XJX	ITE-FOE	DIFF-FOE	PLL
Amplitude	ω_1	0.001	0.004	0.001	0.002	0.003	0.010	0.005
modulation	ω_2	0.001	0.004	0.001	0.002	0.003	0.010	-
Phase	ω_1	0.020	0.006	0.002	0.004	0.048	0.009	0.025
modulation	ω_2	0.246	23.326	23.086	40.526	79.222	15.768	-
Positive	ω_1	0.043	19.579	4.201	25.795	55.027	0.016	0.048
ramp	ω_2	0.637	19.580	4.201	25.795	55.027	0.016	-
Negative	ω_1	0.086	22.696	4.117	24.382	32.778	0.016	0.091
ramp	ω_2	0.635	22.697	4.117	24.382	32.779	0.016	-

This article has been accepted for publication in a future issue of this journal, but has not been fully edited. Content may change prior to final publication. Citation information: DOI 10.1109/TIM.2021.3139652, IEEE Transactions on Instrumentation and Measurement

TABLE XI: MSEs of $\hat{\omega}_0$ with different combinations of 64QAM symbol (unit: dB)

	Proposd Method	UFE Method	BFEL Method	XJX Method	ITE-DFT Method	DIFF-DFT Method	PLL Method
$\{1+j,\ 1+3j\}$	-98.9064	-90.6185	-41.8568	-28.6852	-36.5555	-75.7581	-96.4532
$\{1+j,\ 1+5j\}$	-99.2897	-95.1879	-33.8279	-28.6842	-34.3535	-90.5598	-96.9367
$\{1+j,\ 1+7j\}$	-100.0315	-96.9839	-26.2352	-28.6839	-33.5013	-96.5699	-96.4578
$\{1+j,\ -1-j\}$	-94.9775	-93.7092	-41.4395	-30.0236	-33.4679	-76.3738	-94.7346
$\{1+j,\ -1-3j\}$	-98.6781	-97.5644	-28.8736	-29.5114	-32.8817	-77.8916	-95.3346
$\{1+j,\ -1-5j\}$	-96.2039	-95.8673	-31.3567	-28.0228	-27.5122	-91.1075	-96.0328
$\{1+j,\ -1-7j\}$	-99.7640	-99.6668	-23.8708	-29.2829	-32.5654	-94.2626	-96.7843

VI. Conclusion

The IpDFT algorithm proposed in this paper effectively estimates the frequency of the single tone signal with parameter step change in the sampling signal sequence. The relationship between the DFT bins and the step changed parameters is given by several linear equations. At most six different DFT bins are used to eliminate the effect of the parameter (frequency, amplitude or phase) step change on the L-th sample. The results of simulation and experiment confirm that the proposed algorithm gives precise results. As a future work, we will study an improved method for the multi-frequency signal with multi-symbol step change.

References

[1] Z. Oubrahim, V. Choqueuse, Y. Amirat, and M. E. H. Benbouzid, "Maximum-likelihood frequency and phasor estimations for electric power grid monitoring," *IEEE Trans. Ind. Informat.*, vol. 14, no. 1, pp. 167–177, 2018.

[2] V. Choqueuse, A. Belouchrani, F. Auger, and M. Benbouzid, "Frequency and phasor estimations in three-phase systems: Maximum likelihood algorithms and theoretical performance," *IEEE Trans. Smart Grid*, vol. 10, no. 3, pp. 3248–3258, 2019.

[3] K. Chauhan, M. V. Reddy, and R. Sodhi, "A novel distribution-level phasor estimation algorithm using empirical wavelet transform," *IEEE Trans. Ind. Electron.*, vol. 65, no. 10, pp. 7984–7995, 2018.

[4] S. Reza, M. Ciobotaru, and V. G. Agelidis, "Accurate estimation of single-phase grid voltage fundamental amplitude and frequency by using a frequency adaptive linear kalman filter," *IEEE J. Emerg. Sel. Top. Power Electron.*, vol. 4, no. 4, pp. 1226–1235, 2016.

[5] H. Ahmed, S. Biricik, and M. Benbouzid, "Linear kalman filter-based grid synchronization technique: An alternative implementation," *IEEE Trans. Ind. Informat.*, pp. 1–1, 2020.

[6] H. Ahmed, S. Amamra, and I. Salgado, "Fast estimation of phase and frequency for single-phase grid signal," *IEEE Trans. Ind. Electron.*, vol. 66, no. 8, pp. 6408–6411, 2019.

[7] S. Nam, S. Kang, L. Jing, and S. Kang, "A novel method based on prony analysis for fundamental frequency estimation in power systems," in *IEEE 2013 Tencon - Spring*, 2013, pp. 327–331.

[8] D. Belega, D. Fontanelli, and D. Petri, "Low-complexity least-squares dynamic synchrophasor estimation based on the discrete fourier transform," *IEEE Trans. Instrum. Meas.*, vol. 64, no. 12, pp. 3284–3296, 2015.

[9] D. Belega, D. Fontanelli, and D. Petri, "Dynamic phasor and frequency measurements by an improved taylor weighted least squares algorithm," *IEEE Trans. Instrum. Meas.*, vol. 64, no. 8, pp. 2165–2178, 2015.

[10] P. Romano and M. Paolone, "Enhanced interpolated-dft for synchrophasor estimation in fpgas: Theory, implementation, and validation of a pmu prototype," *IEEE Trans. Instrum. Meas.*, vol. 63, no. 12, pp. 2824–2836, 2014.

[11] A. Derviškadić, P. Romano, and M. Paolone, "Iterative-interpolated dft for synchrophasor estimation: A single algorithm for p- and m-class compliant pmus," *IEEE Trans. Instrum. Meas.*, vol. 67, no. 3, pp. 547–558, 2018.

[12] N. Nevaranta, S. Derammelaere, J. Parkkinen, and B. Vervisch, "Online identification of a mechanical system in frequency domain using sliding dft," *IEEE Trans. Ind. Electron.*, vol. 63, no. 9, pp. 5712–5723, 2016.

[13] X. Yang, J. Zhang, X. Xie, and X. Xiao, "Interpolated dft-based identification of sub-synchronous oscillation parameters using synchrophasor data," *IEEE Trans. Smart Grid*, vol. 11, no. 3, pp. 2662–2675, 2020.

[14] D. Belega, D. Macii, and D. Petri, "Fast synchrophasor estimation by means of frequency-domain and time-domain algorithms," *IEEE Trans. Instrum. Meas.*, vol. 63, no. 2, pp. 388–401, 2014.

[15] D. Macii, D. Petri, and A. Zorat, "Accuracy analysis and enhancement of dft-based synchrophasor estimators in off-nominal conditions," *IEEE Trans. Instrum. Meas.*, vol. 61, no. 10, pp. 2653–2664, 2012.

[16] E. Aboutanios and B. Mulgrew, "Iterative frequency estimation by interpolation on fourier coefficients," *IEEE Trans. Signal Process.*, vol. 53, no. 4, pp. 1237–1242, 2005.

[17] E. Aboutanios, "A modified dichotomous search frequency estimator," *IEEE Signal Process. Lett.*, vol. 11, no. 2, pp. 186–188, 2004.

[18] Y. Dun and G. Liu, "A fine-resolution frequency estimator in the odd-dft domain," *IEEE Signal Process. Lett.*, vol. 22, no. 12, pp. 2489–2493, 2015.

[19] H. Wen, C. Li, and L. Tang, "Novel three-point interpolation dft method for frequency measurement of sine-wave," *IEEE Trans. Ind. Informat.*, vol. 13, no. 5, pp. 2333–2338, 2017.

[20] H. Wen, J. Zhang, Z. Meng, and S. Guo, "Harmonic estimation using symmetrical interpolation fft based on triangular self-convolution window," *IEEE Trans. Ind. Informat.*, vol. 11, no. 1, pp. 16–26, 2015.

[21] J. Sun S. Ye and E. Aboutanios, "On the estimation of the parameters of a real sinusoid in noise," *IEEE Signal Process. Lett.*, vol. 24, 2017.

[22] Y. H. Kim, K. J. Son, S. Kang, and T. G. Chang, "Improved frequency estimation algorithm based on the compensation of the unbalance effect in power systems," *IEEE Trans. Instrum. Meas.*, pp. 1–1, 2020.

[23] T. Tyagi and P. Sumathi, "Frequency estimation based on moving-window dft with fractional bin-index for capacitance measurement," *IEEE Trans. Instrum. Meas.*, vol. 68, no. 7, pp. 2560–2569, 2019.

[24] A. Derviškadić, P. Romano, and M. Paolone, "Iterative-interpolated dft for synchrophasor estimation: A single algorithm for p- and m-class compliant pmus," *IEEE Trans. Instrum. Meas.*, vol. 67, no. 3, pp. 547–558, 2018.

[25] J. Zhang, L. Tang, A. Mingotti, L. Peretto, and H. Wen, "Analysis of white noise on power frequency estimation by dft-based frequency shifting and filtering algorithm," *IEEE Trans. Instrum. Meas.*, vol. 69, no. 7, pp. 4125–4133, 2020.

[26] D. Belega, D. Dallet, and D. Petri, "Accuracy of sine wave frequency estimation by multipoint interpolated dft approach," *IEEE Trans. Instrum. Meas.*, vol. 59, no. 11, pp. 2808–2815, 2010.

[27] D. Belega, D. Dallet, and D. Slepicka, "Accurate amplitude estimation of harmonic components of incoherently sampled signals in the frequency domain," *IEEE Trans. Instrum. Meas.*, vol. 59, no. 5, pp. 1158–1166, 2010.

[28] H. Wen, Z. Teng, and S. Guo, "Triangular self-convolution window with desirable sidelobe behaviors for harmonic analysis of power system," *IEEE Trans. Instrum. Meas.*, vol. 59, no. 3, pp. 543–552, 2010.

[29] D. Kania J. Borkowski and J. Mroczka, "Interpolated-dft-based fast and accurate frequency estimation for the control of power," *IEEE Trans. Ind. Electron.*, vol. 61, no. 12, pp. 7026–7034, 2014.

[30] J. Borkowski, J. Mroczka, A. Matusiak, and D. Kania, "Frequency estimation in interpolated discrete fourier transform with generalized maximum sidelobe decay windows for the control of power," *IEEE Trans. Ind. Inform.*, vol. 17, no. 3, pp. 1614–1624, 2021.

[31] Y. Sun, C. Zhuang, and Z. Xiong, "A scale factor-based interpolated dft for chatter frequency estimation," *IEEE Trans. Instrum. Meas.*, vol. 64, no. 10, pp. 2666–2678, 2015.

[32] Y. Sun, C. Zhuang, and Z. Xiong, "A switch-based interpolated dft for the small number of acquired sine wave cycles," *IEEE Trans. Instrum. Meas.*, vol. 65, no. 4, pp. 846–855, 2016.

[33] K. Wang, H. Wen, and G. Li, "Accurate frequency estimation by using three points interpolated dft based on rectangular window," *IEEE Trans. Ind. Informat.*, pp. 1–1, 2020.

[34] K. Wang, H. Wen, W. Tai, and G. Li, "Estimation of damping factor and signal frequency for damped sinusoidal signal by three points interpolated dft," *IEEE Signal Process. Lett.*, vol. 26, no. 12, pp. 1927–1930, 2019.

[35] K. Wang, H. Wen, L. Xu, and L. Wang, "Two points interpolated dft algorithm for accurate estimation of damping factor and frequency," *IEEE Signal Process. Lett.*, vol. 28, pp. 499–502, 2021.

[36] K. Wang, L. Zhang, H. Wen, and L. Xu, "A sliding-window dft based algorithm for parameter estimation of multi-frequency signal," *Digit. Signal Prog.*, vol. 97, pp. 102617, 2019.

[37] S. Ando, "Frequency-domain prony method for autoregressive model identification and sinusoidal parameter estimation," *IEEE Trans. Signal Process.*, vol. 68, pp. 3461–3470, 2020.

[38] "IEEE 802, ieee p802.11ax/d0.4," 2016.

[39] "IEEE standard for information technology, part 11: Wireless lan medium access control (mac) and physical layer (phy) specifications," .

[40] Y. Liu, Y. Peng, S. Wang, and Z. Chen, "Improved fft-based frequency offset estimation algorithm for coherent optical systems," *IEEE Photonics Technol. Lett.*, vol. 26, no. 6, pp. 613–616, 2014.

[41] J. Han, W. Li, Z. Yuan, and Y. Zheng, "A simplified implementation method of *m* th-power for frequency offset estimation," *IEEE Photonics Technol. Lett.*, vol. 28, no. 12, pp. 1317–1320, 2016.

[42] "Ieee standard for synchrophasor measurements for power systems," *IEEE Std C37.118.1-2011 (Revision of IEEE Std C37.118-2005)*, pp. 1–61, 2011.

[43] "Ieee standard for synchrophasor measurements for power systems – amendment 1: Modification of selected performance requirements," *IEEE Std C37.118.1a-2014 (Amendment to IEEE Std C37.118.1-2011)*, pp. 1–25, 2014.

[44] M. Karimi-Ghartemani, M. Mojiri, A. Safaee, and J. A. Walseth, "A new phase-locked loop system for three-phase applications," *IEEE Trans. Power Electron.*, vol. 28, no. 3, pp. 1208–1218, 2013.

[45] F. Baradarani, M. R. Dadash Zadeh, and M. A. Zamani, "A phase-angle estimation method for synchronization of grid-connected power-electronic converters," *IEEE Trans. Power Deliv.*, vol. 30, no. 2, pp. 827–835, 2015.

[46] J. Ren and M. Kezunovic, "Real-time power system frequency and phasors estimation using recursive wavelet transform," *IEEE Trans. Power Deliv.*, vol. 26, no. 3, pp. 1392–1402, 2011.

[47] J.Xiao, J.Feng, J.Han, and W.Li, "Low complexity fft-based frequency offset estimation for m-qam coherent optical systems," *IEEE Photonics Technol. Lett.*, vol. 27, no. 13, pp. 1371–1374, 2015.

[48] A. Peng, G. Ou, and M. Shi, "Frequency estimation of single tone signals with bit transition," *IET Signal Process.*, vol. 8, pp. 1025–1031, 2014.

[49] J. Han, W. Li, J. Xiao, and J. Feng, "Frequency offset estimation with multi-steps interpolation for coherent optical systems," *IEEE Photonics Technol. Lett.*, vol. 27, no. 19, pp. 2011–2014, 2015.

[50] J. Lu, Y. Tian, S. Fu, and X. Li, "Frequency offset estimation for 32-qam based on constellation rotation," *IEEE Photonics Technol. Lett.*, vol. 29, no. 23, pp. 2115–2118, 2017.

[51] Ž. Zečević, B. Krstajić, and T. Popović, "Improved frequency estimation in unbalanced three-phase power system using coupled orthogonal constant modulus algorithm," *IEEE Trans. Power Deliv.*, vol. 32, no. 4, pp. 1809–1816, 2017.

[52] "https://www.ni.com/zh-cn/shop/software/products/rfmx-wlan.html," .